

Particle-laden viscous thin-film flows on an incline: experiments compared with a theory based on shear-induced migration and particle settling

N. Murisic^a, J. Ho^b, V. Hu^c, P. Latterman^d, T. Koch^e, K. Lin^f, M. Mata^a, A. Bertozzi^a

^aMathematics Department, University of California, Los Angeles, CA 90095, USA

^bDepartment of Chemical and Biomolecular Engineering, University of California, Los Angeles, CA 90095, USA

^cMechanical and Aerospace Engineering Department, University of California, Los Angeles, CA 90095, USA

^dDepartment of Bioengineering, University of California, Los Angeles, CA 90095, USA

^eDepartment of Physics, Harvey Mudd College, Claremont, CA 91711, USA

^fDepartment of Mathematics, The University of Hong Kong, Pokfulam, Hong Kong

Abstract

Particle settling in driven viscous films is a complex physical process involving different physical effects. A recent analysis in [1] identified a balance between hindered settling and shear-induced migration as the dominant large scale physics for particle/liquid separation. However, experimental data for this has been lacking. This paper presents new data including the role of particle size and liquid viscosity showing clear agreement with the theory. We discuss the role of timescales in the dynamics of the experiment and present results from a dynamic model.

Key words: thin films, particle-laden flows, fingering instability, shear-induced migration

PACS: 47.15.gm, 47.55.Kf, 83.80.Hj

1. Introduction and background

Particle-laden flows in general are important in a variety of contexts, including environmental, industrial and biological ones, where transport and manipulation of suspensions occur. Specific examples are mud flows, debris flows, slurry transport, food processing, various coating processes in ceramics and electronics industries, and manufacturing processes in pharmaceutical and paper industries, where uniformity in particle distribution is usually required. While many studies in the literature address gravity-driven clear liquid flows (e.g. see [2, 3, 4, 5, 6, 7]) and pure granular flows (e.g. [8, 9, 10]), comparatively fewer studies have centered on particle-laden thin film flows [1, 11, 12, 13]. Apart from complexities associated with moving contact lines, the study of slurries also involves an intricate interplay between particle settling/migration and viscous fingering mechanisms.

1.1. Settling of particles due to gravity

The settling of particles in quiescent liquids and sedimentation in suspensions have also garnered significant attention (e.g. see [14, 15, 16, 17, 18, 19]). For rigid spherical particles, the well-known Stokes' Law applies, neglecting inertial effects of the liquid due to the smallness of Reynolds number. In order to account for the presence of a large number of identical particles, the velocity given by Stokes' Law is typically modified by a purely empirical multiplicative hindrance function which depends on particle volume fraction, ϕ . This function, typically denoted by $f(\phi)$, has been a matter of much discussion through the decades. In [14], a so-called Richardson-Zaki expression was proposed, where $f(\phi) \sim (1 - \phi)^m$, with $m \approx 5.1$, and found

to compare favorably with experimental data for moderately dilute suspensions. For dilute dispersions, $f(\phi) \sim (1 - 6.55\phi)$ was suggested in [15]. Other, more complex expressions for $f(\phi)$ were discussed in [16, 17, 18] and [19]. In the presence of shear, a hindrance function of form $f(\phi) \sim (1 - \phi)$ was shown to be appropriate in [20].

1.2. Shear-induced migration of particles

Concentrated suspensions of spherical particles have been shown to behave curiously when subjected to shear. This phenomena was first detected in experiments with Couette viscometer, where unusual decrease in measured viscosity occurred during prolonged shearing. The theoretical framework for this phenomena was laid out in [21, 22] and subsequently rephrased in [23]. Its key element was *shear-induced migration*, a diffusive mechanism resulting from gradients in both particle volume fraction and suspension viscosity, $\mu(\phi)$. Net fluxes caused by these gradients were deduced by considering irreversible interactions between pairs of smooth spherical particles (for details, see [22]). In [23], the predictions of this model were shown to be in excellent agreement with experimental data for Couette flows, and the use of the model was also extended to flows of concentrated suspensions through cylindrical tubes. Recently, the model was employed in [24] to carry out numerical simulations for suspension flows in more complex geometries. Other studies, focusing on migration of particles in pressure-driven channel flows [25], steady and unsteady flows in various geometries [26], and inclined free-surface channel flows [27], were carried out using a different approach, inspired by Stokesian Dynamics. In particular, in [25] and [26],

the coupling between particle mass and momentum conservation was analyzed, whereby particles migrated due to the requirements of the momentum balance when normal forcing is exerted by neighboring particles. We note that, at least for the set-up we consider here, the migration flux resulting from this alternate approach turns out to be similar to the one based on the diffusive mechanism.

1.3. Particle-laden thin film flows

More recent studies addressed particle-laden thin film flows with contact lines. Zhou *et. al* [11] reported on their preliminary experimental results for incline flows of suspensions of polydisperse glass beads with diameter $\sim O(100\mu\text{m})$, focusing on a single bead size. As they varied the bulk particle volume fraction, ϕ_0 , and the inclination angle, α , they identified three distinct settling regimes: for small ϕ_0 and α values, the particles would settle out of the flow, clear liquid film would flow over the particulate bed and the fingering instability resulted; for large values of ϕ_0 and α , the particles would move faster than the liquid, leading to aggregation of particles in the contact line region, formation of particle-rich ridge, and almost complete suppression of the fingering instability; finally, intermediate values of these parameters would lead to a well-mixed regime in which fingering instability occurred. A theoretical model was also derived in [11], based on the Navier-Stokes equations for the liquid and a diffusive model for particle volume fraction, including capillary effects and hindered settling. A simplified version of this model, which neglected higher order capillary terms was studied in a shock dynamics framework in [11] and [12]. Although successful in explaining qualitatively the formation of the particle-rich ridge, they did not provide a quantitative model nor did they ever attempt to model the other regimes. In an effort to improve understanding of these regimes, Cook [1] included shear-induced migration in his model. He assumed that the outcome of particle settling is guided by the balance between shear-induced migration and hindered settling. Through his steady state formulation, he derived a system of ODEs for ϕ and shear stress, σ . However, this model did not include a hindrance effect due to the presence of the solid track. Furthermore, while he found good agreement between model's predictions regarding well-mixed regime and the experimental data, the data itself was from [11] – old, preliminary and rather limited. Additional work in [13] focused on studying the propagation of contact lines in particle-laden thin film flows experimentally. We note that this work only focused on the well-mixed and particle ridge regimes and did not focus on the transitions studied by Cook [1], but rather on the dynamics of the front. Apart from varying ϕ_0 and α , particle size and density, and liquid viscosity were all varied in order to examine their influence on the front speed. It was found that the dependence of the front position on time was of power-law type, with exponents similar to 1/3 proposed in [2].

1.4. The objectives

The two papers discussed at the end of the last section, namely [1] and [13], suggest key important points for further

study. Cook's paper [1] suggests that the balance between shear-induced migration and particle settling may be important in understanding a broad range of dynamics of particle laden flows. However, given the lack of experimental data in that paper, more detailed experiments are needed showing the role of particle size and fluid viscosity on the settling behavior, to better understand the importance of this physical balance. In this work we carry out a systematic experimental study of settling regimes over a range of particle sizes and liquid viscosities. Through comparison between our experimental results and the predictions of equilibrium theory, we uncover the transient nature of the well-mixed regime, where bifurcation to either of the remaining regimes eventually occurs. In addition, our experimental results clearly indicate how the particle size and the liquid viscosity affect the timescale on which we observe this transient regime. These results point towards a new dynamic model that might better explain some of the departures from clear fluid behavior observed in the experiments by Ward *et. al.* [13]. We discuss a possible way to incorporate this physics into a dynamic continuum model and discuss mathematical issues associated with this model.

In contrast to the preliminary experimental results from [11], which included only a few experiments with a single particle/silicon oil combination, we perform thorough experiments with three different particle sizes and two different liquid types, and vary ϕ_0 and α over wide ranges of values, in order to study the influence of these two material parameters on the settling regime. The liquid viscosity and the particle size are found to affect the width of the region in (ϕ_0, α) -space over which the transition between settled and ridged regimes occurs. Therefore, we show that these parameters dictate both the likelihood of observing the well-mixed regime for given ϕ_0 and α values, and the timescale over which the well-mixed suspension is preserved. We also present an argument based on a competition between two relevant times scales which qualitatively explains the connection between particle size and the well-mixed regime. This role of particle size has not been documented in the literature. Next, we derive a theoretical model. We consider the steady state of the system where hindered settling balances the shear-induced migration of particles. Our modeling approach is similar to the one in [1], with one difference: we also include the hinderance to settling due to the presence of the solid track. We show excellent agreement between model's predictions and our experimental results over all ranges of viscosities and particle sizes. Furthermore, we show how the results of numerical simulations of our model provide additional evidence for transiency of well-mixed regime. The experimental data shows a clear dependence of the different flow regimes on particle size. Most notably, the well-mixed regime occurs over a wider range of inclination angles and particle concentrations for smaller sized particles. We explain this by examining the respective timescales associated with the motion of the front on the track versus the timescale of particle settling. Dimensional analysis of these timescales provides a good qualitative understanding of this behavior. Finally, we derive a dynamic model inspired by the flux balance from the equilibrium theory. We show preliminary numerical simulations that exhibit

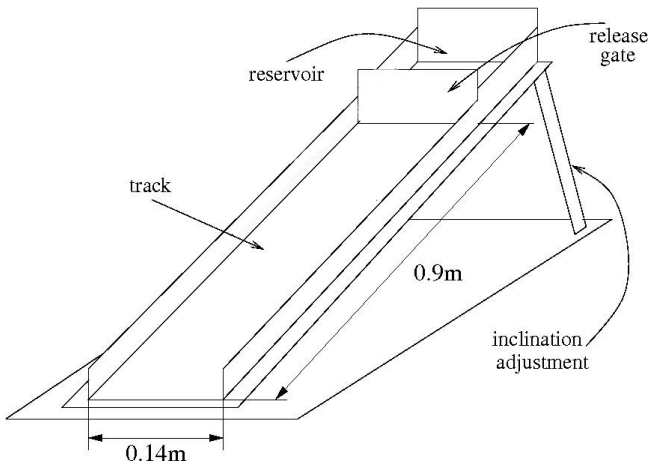


Figure 1: The experimental apparatus.

the same dynamic behavior observed in the experiment. We discuss interesting findings regarding conditional hyperbolicity of the resulting system.

This paper is organized as follows. In §2 we describe our experimental set-up, list material parameters and identify the techniques employed in collecting data. This is followed by a discussion of our experimental results in §3, and the outline of the derivation of the equilibrium model in §4. Also in §4, we compare the predictions of the model with the experimental results. In §5 we present a dimensional analysis of relevant timescales and compare theoretical predictions of these timescales with the experimental data, in particular the dependence of the well-mixed regime on particle size. Next, we discuss a possible dynamic model for particle-laden thin film flows in §6. Finally, we summarize our findings and discuss challenges in going from equilibrium to full dynamic theory in §7.

2. Experimental apparatus and techniques

Figure 1 shows the experimental apparatus we use. It consists of a steel base platform and an acrylic track, with adjustable inclination angle, α (range: $5^\circ - 80^\circ$). The track is 0.9 m long and 0.14 m wide, with 0.02 m side walls. A liquid/particle mixture prepared beforehand is poured into the reservoir situated at the top of the track (reservoir dimensions: $height \times width \times length = 0.04 \times 0.14 \times 0.1$ m) and the gate is lifted, allowing it to flow down the track, with the contact line initially straight. Here, we only focus on experiments with finite, constant suspension volume. The evolution of the flow is monitored using a digital camera, which is positioned above the track and captures images of the moving front at predetermined time intervals, typically 0.25 – 4 s. Using this setup, we are able to monitor the film motion, starting from release, until the front has reached approximately 0.6 m down the track (few additional images of the flow are taken just before the contact line reaches the lower end of the track). Several fluorescent

	ν (m^2/s)	ρ_l (kg/m^3)	ρ_p (kg/m^3)	d (mm)
L1	10^{-4}	966	–	–
L2	10^{-3}	971	–	–
P1	–	–	2475	0.143
P2	–	–	2475	0.337
P3	–	–	2475	0.625

Table 1: Physical properties of liquids and particles used in the experiments.

	P1	P2	P3
L1	Experiment C	Experiments A,C	–
L2	Experiment B	Experiments A,B	Experiment B

Table 2: Different liquid/particle combinations we consider. We study the manner in which viscosity of suspending liquid (Experiment A) or particle size (Experiments B and C) affects the settling regime.

lights are placed below the track for imaging purposes, while food-coloring dye is employed to enhance contrast. Images are subsequently analyzed, and each experimental run is classified, based on observed settling regime, as either ‘settled’, ‘well-mixed’ or ‘ridged’ (see §3 for details).

Our experiments involve three different particle types and two different liquids. The particles are smooth spherical glass beads (Ceroglass), and we consider three different diameters: $d = 0.143$ mm (‘P1’), 0.337 mm (‘P2’), and 0.625 mm (‘P3’). The standard deviation of particle diameters is 26% for all particle sizes. For suspending liquid, we use polydimethylsiloxane (PDMS) (AlfaAesar) in two different kinematic viscosities: $\nu = 10^{-4}$ m^2/s (‘L1’) and 10^{-3} m^2/s (‘L2’). The particles are heavy, i.e. $\rho_p > \rho_l$ for all particle and liquid types, where ρ_p and ρ_l are particle and liquid densities respectively. Relevant material parameters are summarized in Table 1.

Suspensions are prepared by first weighing the particles and PDMS individually, pouring PDMS into a container, and then adding particles; slow manual stirring is used until uniform mixture is obtained. This procedure prevents formation of air bubbles. Typically, no haste is required between the preparation of suspension and its release down the track since uniformity of the mixture is preserved for sufficiently long time-intervals. The settling which occurs in the sample before it is released is negligible. The bulk volume fraction of particles, ϕ_0 , is defined as $\phi_0 = V_p/V$, where $V = V_l + V_p$ is the total volume of the mixture, and V_l and V_p are liquid and particles volumes respectively. Here, we focus on V between 75 ml and 103 ml.

The experiments are carried out in open air and at room temperature (298 K), maintained by the air-conditioning unit. The fluorescent lights we use for imaging purposes radiate heat, but the amount is insufficient to affect either viscosity of liquid, flow dynamics, or observed particle behavior in any significant manner. The track, gate and reservoir are cleaned after each experimental run using a squeegee to remove the excess particulate and dust which may accumulate. Although this cleaning procedure does not remove PDMS entirely, it ensures reproducibility of our experimental results.

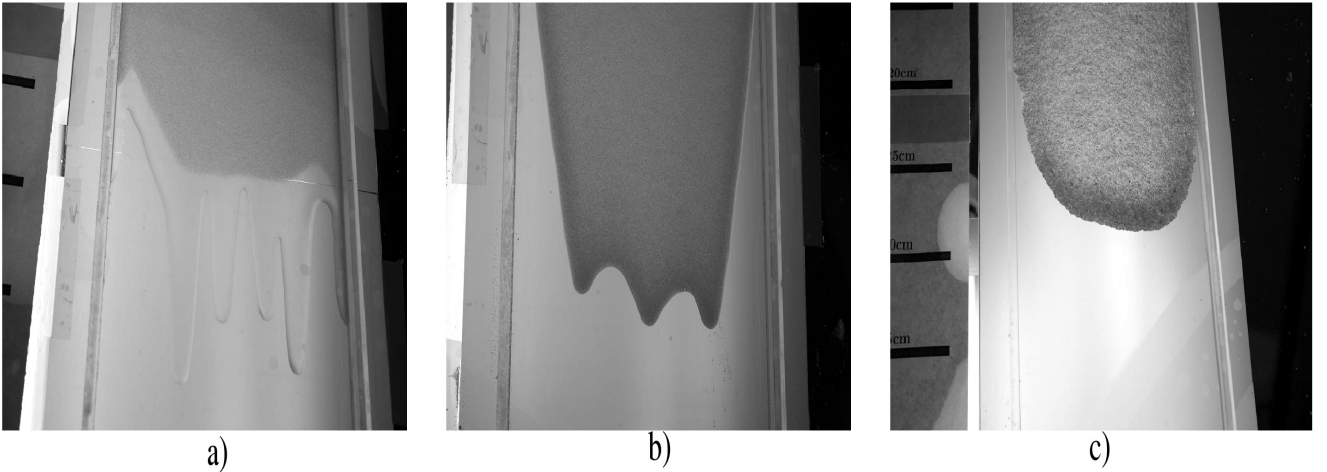


Figure 2: The settling regimes: a) settled; b) well-mixed; and c) ridged. The fingering instability typical to clear liquid flows is *only* observed in settled and well-mixed regimes.

We carry out three different sets of experiments, conveniently summarized in Table 2. In all experiments, we vary ϕ_0 between 0.25 and 0.50, and α between 20° and 50° . In Experiment A, we consider medium-sized particles, P2, and both PDMS types in order to study the influence of the viscosity of suspending liquid on the settling regime. Experiments B and C focus on studying the influence of particle size, by fixing the liquid type (L2 in B and L1 in C) and varying the particle size. When L1 PDMS and P3 particles are used, rapid settling occurs. Regardless of our best efforts, significant fraction of particles often settles to the bottom of the reservoir before suspension is ever released down the track. Hence, we omit experiments with this mixture.

3. Experimental results

In all experiments, the observed flows are relatively slow. In addition, settling behavior can only be classified after an initial transient stage which typically lasts up to 900 s. The settling regimes observed in our experiments resemble the ones discussed in [11]: each experimental run is labeled as either settled, well-mixed, or ridged. Typical examples of these regimes are shown in Fig. 2. In general, these three regimes occur in each experimental set, A, B and C (an exception is discussed below).

In settled regime, the particles tend to quickly settle out of the flow, forming a particulate bed, with the suspending liquid moving down the track faster than particles. Virtually clear liquid film ultimately leaves the particulate bed far behind and develops the fingering instability as described in [2]. The particulate bed moves down the incline slowly until the end of the experiment, its front remaining stable. Typically, this regime occurs for small values of ϕ_0 and α . In contrast, when ϕ_0 and α are large, the particles move faster than suspending liquid, they aggregate in the contact line region, forming a particle-rich ridge, often several times thicker than trailing film. Hence, we refer to this regime as ridged. The large volume fraction of particles at the front appears to suppress the fingering instability. We do not

measure the local particle volume fraction in our experiments. However, we suspect that in this regime its value at the free surface is close to the maximum packing, but slightly smaller since we rarely encounter solid-like behavior for the range of parameters considered here. Intermediate values of ϕ_0 and α lead to well-mixed regime, where volume fraction of particles remains almost uniform throughout the film. The fingering instability occurs, but compared to settled regime, it is typically characterized by longer wavelength.

Initially, as the mixture is released from the reservoir, the observed flow is unsteady. However, as the front moves down the track, the flow typically becomes fully developed (it reaches a quasi-steady state where downstream variations are not important to the leading order). The distance from the release gate at which this occurs varies depending on the liquid/particle combination used; in most of our experimental runs this happens while the front is in the zone where high frequency images are taken ($< 0.6 m$ down the track); beyond this point on the track, the unsteady transitions between settling regimes occur only when lower viscosity PDMS/smaller particles are used, and only in a few runs the front reached the end of the track without the flow becoming fully developed (all such runs are with the lowest viscosity PDMS/smallest particles combination). Indeed, this observation agrees with the experimental and numerical results from [27], concerning free-surface channel flows in the case of density matched particles suspended in ethanol-based liquids (with the liquid viscosity and particle size similar to the L2/P1 mixture, and $\alpha = 33.5^\circ$). In particular, based on their results, one expects all our runs to exhibit fully developed flows before the end of the track is reached, save perhaps for runs involving L1 and P1 or P2, when $\phi_0 < 0.3$. The flow details of each run are analyzed based on captured images; the classification of each run (settled, well-mixed, or ridged) is carried out based on recorded behavior throughout the entire run, with emphasis on the images of the flow as the front closes in on the end of the track (0.6 m from the release gate and beyond). For any particular liquid/particle combination,

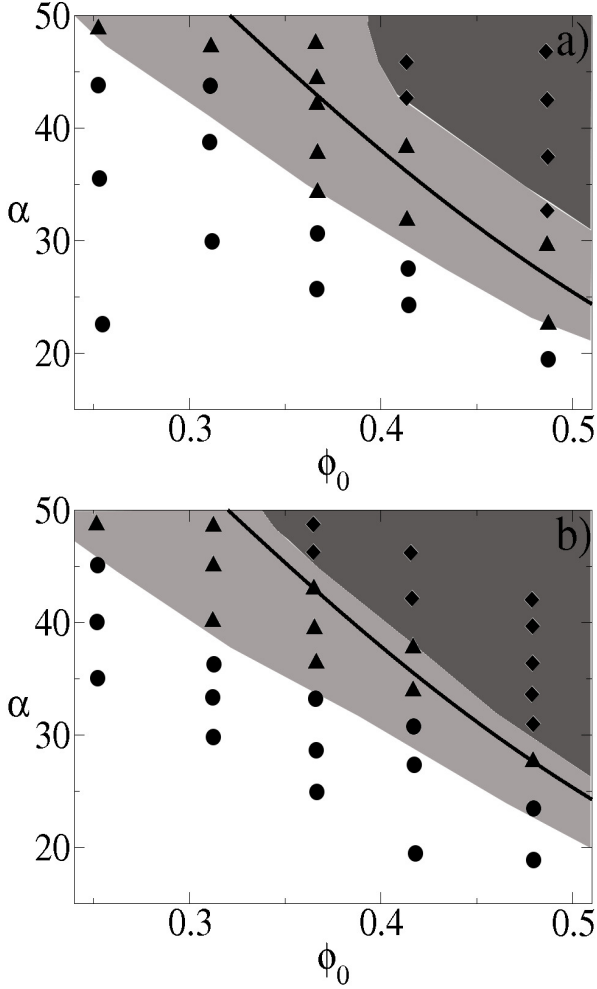


Figure 3: Phase diagrams for Experiment A. Particle type is fixed (P2), viscosity of suspending liquid is varied: a) low (L1); and b) high (L2). Symbols denote regimes observed in experimental runs: circles (●) for settled, triangles (▲) for well-mixed, and diamonds (◆) for ridged. The solid curve represents prediction of the equilibrium model (see §4) for a regime where $\phi' = 0$ (well-mixed).

we classify each experimental run and compile the results of the classification in a corresponding (ϕ_0, α) phase diagram (see Figs. 3, 4 and 5). These diagrams show distinct bands of settling behavior. We use color to label these bands: *white* for settled, *light* for well-mixed, and *dark* for ridged. Boundaries between different regime bands are determined based on the behavior recorded in images (i.e., the details of the flow) for each experimental run. Figures 3, 4 and 5 each include a solid black curve superposed on the experimental results. These curves represent a well-mixed regime prediction (i.e. $\phi' = 0$, where $\phi(z)$ is particle volume fraction) of the equilibrium model. The discussion regarding the model and the agreement between its predictions and the experimental results is given in §4.

We note that other more complex behavior also occurs. In some experimental runs, we notice capillary motion of particles along the side walls or their alignment in linear streaks along the track. Irregularities in shape and size of fingers, and extreme cases of ridged regime, where sections of contact line

experience jamming with particles, become solid-like and virtually break off in blocks are also observed. These phenomena are attributed to either finite width of track and presence of side walls or complex interplay between particle migration and contact line effects. While very intriguing, we leave detailed study of such complex behavior for future work, and focus here on three settling regimes described above.

We proceed by discussing dependence of settling behavior on viscosity of suspending liquid and particle size by presenting results of Experiments A, B and C.

3.1. Experiment A: influence of viscosity of suspending liquid

In Experiment A, we consider intermediate size particles, P2, and both the low and the high viscosity liquid (L1 and L2 respectively). This allows us to study the dependence of observed settling behavior on PDMS viscosity. Since, based on Stokes' Law (e.g. see [15]), the settling velocity of particles is inversely proportional to liquid viscosity, a decrease in PDMS viscosity should result in enhanced tendency of particles to settle out of the flow. Figure 3 shows phase diagrams which result for low, a), and high viscosity, b).

At a first glance, the outcomes appear to be rather similar for the two liquids, although the band for the settled regime is somewhat wider in Fig. 3a) compared to b), confirming our expectations based on the settling time. A closer inspection also reveals that the well-mixed band is wider when the viscosity of the suspending liquid is lower (Fig. 3a)). In order to better understand this difference, we consider the timescales of the motion of the front and the settling of the particles. For clear liquid inclined flows, the former timescale is proportional to the viscosity of the liquid, μ (e.g. see [11]). However, for suspensions $\mu = \mu(\phi)$. For estimation purposes, we may assume uniformity of the slurry (i.e. well-mixed case), and by using the Krieger-Dougherty relation, $\mu(\phi) = \mu_l(1 - \phi/\phi_{max})^{-2}$ as in [28, 29], we get that this timescale is proportional to $\mu_l = \rho_l \nu$, the viscosity of the suspending liquid; here, ϕ_{max} denotes maximum packing volume fraction. It is now clear that a decrease in the viscosity of the suspending liquid, with all the other material parameters fixed, leads to a faster propagation of the suspension front. On the other hand, for purely gravity driven particle settling, the relevant timescale is viscous and also directly proportional to μ_l (see §4) – a decrease in viscosity leads to a faster settling of particles. Therefore, if gravity were the only mechanism responsible for particle settling, the width of the well-mixed bands in Fig. 3 would have been independent of the viscosity. The fact it is not, suggests that some part of the relevant settling dynamics occurs on a timescale other than the viscous one. In §4, we conjecture that the settling behavior is governed by a balance between the settling due to gravity and the shear-induced migration. This balance may lead to a settling which occurs on a different timescale, introducing a correction to the pure viscous one. Accordingly, while a decrease in the viscosity clearly affects the motion of the front, it may only have a relatively minor effect on the settling rate. Hence, due to the finite length of the track used in the experiments, the suspensions with low viscosity PDMS are likely to run out of track length before the final state of the system has been achieved. As a result, some runs

which, given a longer track, would eventually become settled or ridged, are classified as well-mixed. This argument not only explains the differences between Figs. 3a) and b), but also gives a hint regarding the nature of the well-mixed regime: it appears to be an intermediate transient state of the system that eventually, given a sufficient time, bifurcates to either the settled or the ridged regime. The notion of transiency of the well-mixed regime is discussed in more detail in §5.

3.2. Experiments B and C: influence of particle size

Next, we examine the manner in which particle size affects the settling regime. For this purpose, we carry out Experiments B and C, where liquid type is fixed and particle size is varied.

In Experiment B, we consider high viscosity suspending liquid, L2, and all three particle sizes, P1, P2, and P3 (note: experimental runs with L2/P2 combination have already been carried out in Experiment A). According to Stokes' Law, the settling velocity is proportional to d^2 , and hence, largest particles are most likely settle out of the flow. Based on this reasoning, the settled band should be widest for P3. The phase diagrams resulting from Experiment B are shown in Fig. 4.

Compared to Experiment A, the differences between different diagrams are much more pronounced. The speculation based on Stokes' Law is again proven correct – compared to Figs. 4a) and b), the band corresponding to settled regime is widest in Fig. 4c); it is narrowest for smallest particles in Fig. 4a). But, the most striking feature here is a complete absence of well-mixed regime for largest particles in Fig. 4c) – all considered runs with L2/P3 configuration resulted in either settled or ridged behavior. In addition, we notice that the well-mixed band is significantly wider for smallest particles in Fig. 4a) compared to intermediate ones in Fig. 4b). Hence, the trend is obvious: for a fixed liquid viscosity, an increase in particle size makes the well-mixed outcome less likely. This result further supports our hypothesis regarding the transient nature of well-mixed regime. In particular, the diffusive fluxes of particles due to hindered settling and shear-induced migration are both proportional to d^2 (see §4). Since these are, in our opinion, the two main mechanisms of particle motion in the system we study, the smallest particles P1 are moving on a timescale much longer than larger particles P2 and P3. Consequently, and as seen in Fig. 4a), many runs involving P1 remain well-mixed for the duration of the experiment. We suspect that given a longer track and larger sample volume, majority of these flows would eventually bifurcate to either settled or ridged regime. On the other hand, the largest particles P3 move on shorter timescale compared to both P1 and P2. Therefore, the flows involving particles P3 quickly bifurcate to either settled or ridged. The complete absence of well-mixed band in Fig. 4c) serves as an indicator of just how rapid this process is.

Finally, in Experiment C, we study the influence of particle size on the settling behavior for low viscosity PDMS, L1. We focus on small and intermediate size particles, P1 and P2. As discussed in §2, we do not consider the L1/P3 combination since particles in all suspensions of that type undergo rapid settling while still in the reservoir. We also note that the ex-

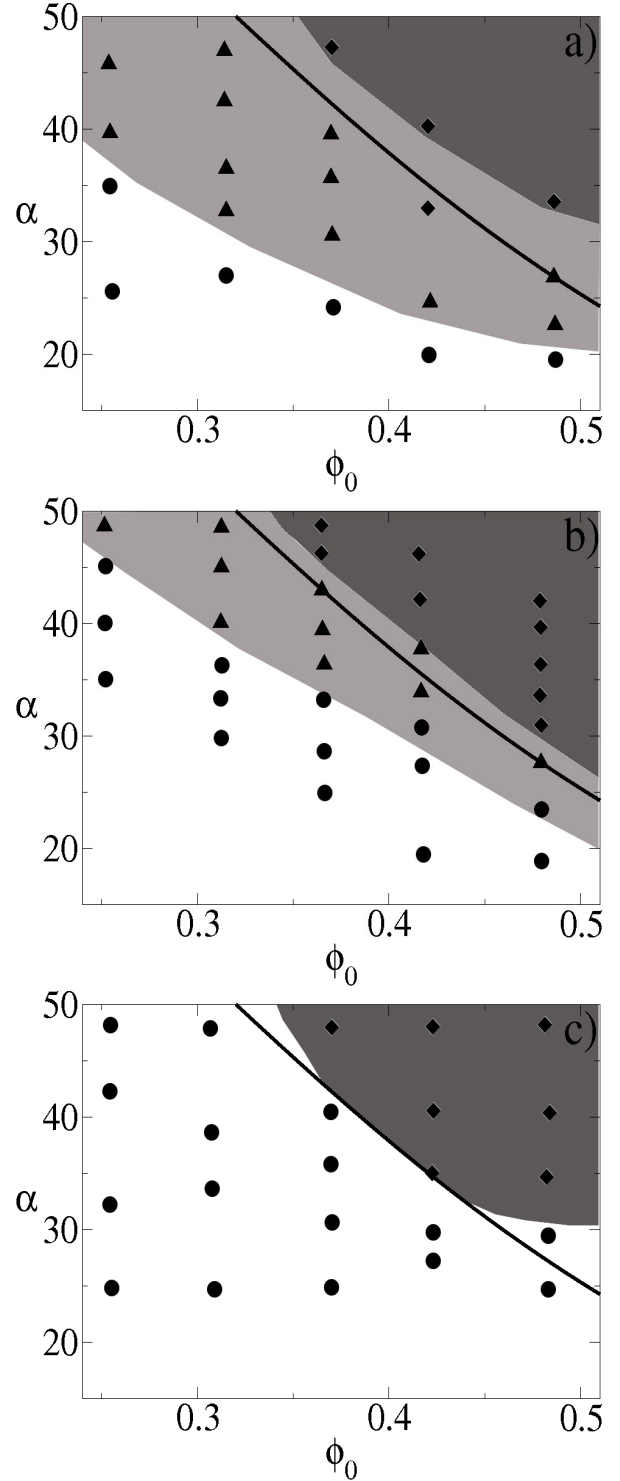


Figure 4: Phase diagrams for Experiment B. Viscosity of suspending liquid is fixed (high viscosity, L2), particle size is varied: a) small (P1); b) intermediate (P2); and c) large (P3). Symbols denote regimes observed in experimental runs: circles (●) for settled, triangles (▲) for well-mixed, and diamonds (◆) for ridged. The solid curve represents prediction of the equilibrium model (see §4) for a regime where $\phi' = 0$ (well-mixed).

perimental runs with the L1/P2 combination have already been carried out in Experiment A.

The results of Experiment C are shown in Fig. 5. The trend observed in Experiment B is quite noticeable here too: as the particle size increases, the uniformity of the suspension is less likely to be preserved. In particular, the well-mixed band is significantly wider in Fig. 5a) compared to the one in b). The explanation for this trend is identical to one for Experiment B. For small particles, the timescale of particle settling is much longer than for larger ones; therefore, uniformity of suspension is likely to be preserved longer for small particles. Furthermore, a comparison of diagrams in Figs. 3, 4 and 5 reveals that the well-mixed regime is more likely to occur for L1/P1 than for any other liquid/particle combination we consider – the well-mixed band in Fig. 5a) is by far the widest. This is particularly evident when Figs. 4a) and 5a) are compared (small particle size, high and low viscosity suspending liquid respectively). The latter comparison also shows that for smallest particles, the influence of viscosity on both prolonging the transient phase and making it more likely for wider range of ϕ_0 and α values is much more pronounced than in Experiment A.

To summarize, Experiments A, B and C show that particle size particularly affects the settling behavior. It dictates the likelihood of occurrence of settled regime and the timescale for the motion of the particles in general. The viscosity of the suspending liquid also influences the particle motion, with its influence increasing as the particle size decreases. The influence of the particle size and the liquid viscosity on the settling outcome is a novel effect, which has not been captured in any previous experiments. Furthermore, our experiments provide another novel result: they reveal the transient nature of the well-mixed regime. This is evident from the manner in which both particle size and viscosity of the suspending liquid affect the persistence of the well-mixed regime. We argue that given a longer track length, a majority of, if not all, well-mixed flows would bifurcate to either the settled or the ridged regime.

4. Theoretical model

We consider a continuum model for particle volume fraction, ϕ . The dynamics of ϕ are described by a conservation equation for particles, written in Eulerian reference frame

$$\frac{D\phi}{Dt} = -\nabla \cdot (\mathbf{J}_{bd} + \mathbf{J}_{grav} + \mathbf{J}_{coll} + \mathbf{J}_{visc}). \quad (1)$$

Here t denotes time, and $D/Dt = \partial/\partial t + \mathbf{v} \cdot \nabla$, where $\mathbf{v} = (\mathbf{u}, \mathbf{w})$; u and w are components of liquid velocity vector \mathbf{v} in x -direction (down the track) and z -direction (normal to track) respectively. Equation 1 includes hindered settling (\mathbf{J}_{grav}), and shear-induced migration effects (\mathbf{J}_{coll} and \mathbf{J}_{visc}). It also includes Brownian diffusive flux, $\mathbf{J}_{bd} = -D\nabla\phi$. We note that since the Péclet number corresponding to our problem is large (i.e. $Pe = \dot{\gamma}d^2/D \sim O(10^3)$, where $\dot{\gamma}$ is magnitude of the local shear rate), henceforth we neglect this effect. The viscosity of the suspension is a function of particle volume fraction, $\mu = \mu(\phi)$. Here, we use the expression from [28, 29], $\mu(\phi) = \mu_l(1 - \phi/\phi_{max})^{-2}$, known

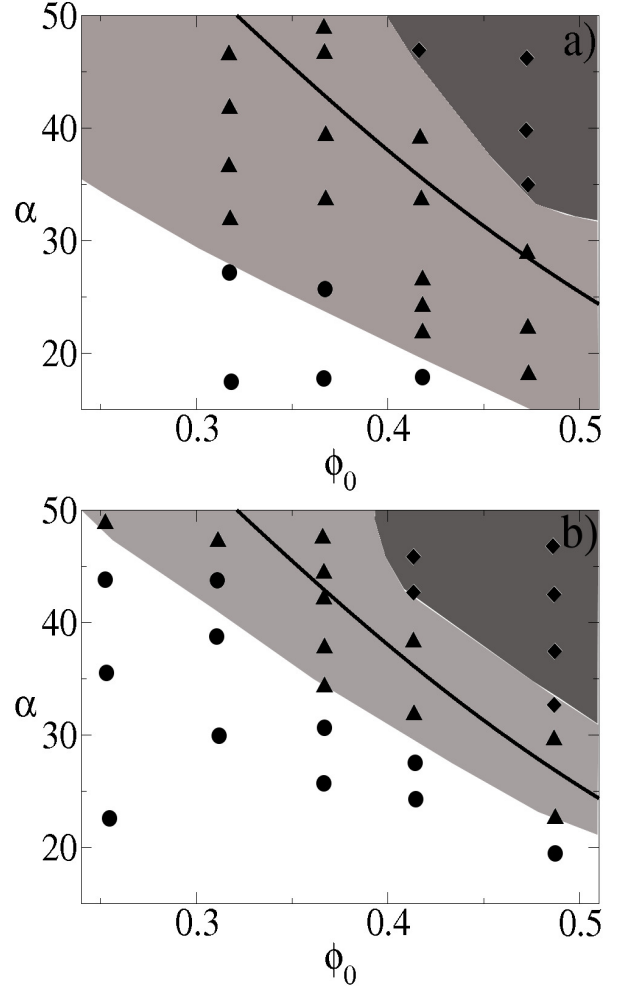


Figure 5: Phase diagrams for Experiment C. Viscosity of suspending liquid is fixed (low viscosity, L1), particle size is varied: a) small (P1) and b) intermediate (P2). Symbols denote regimes observed in experimental runs: circles (●) for settled, triangles (▲) for well-mixed, and diamonds (◆) for ridged. The solid curve represents prediction of the equilibrium model (see §4) for a regime where $\phi' = 0$ (well-mixed).

as the Krieger-Dougherty equation, where ϕ_{max} denotes maximum packing volume fraction, and restricts the meaningful interval of values for ϕ to $[0, \phi_{max}]$, with the mixture becoming almost solid-like as $\phi \rightarrow \phi_{max}$. Different values of ϕ_{max} have appeared in the literature, usually within the range 0.57-0.68 (e.g. see [1, 13, 17, 19, 20, 22, 23, 26, 27]). We use the procedure described in [13] and obtain $\phi_{max} \approx 0.61$.

The settling of a particle due to gravity is hindered by the presence of other particles and the solid track/wall [11]. The net flux of particles caused by this effect is given by

$$\mathbf{J}_{grav} = -\frac{d^2\phi(\rho_p - \rho_l)}{18\mu_l} f(\phi)\omega(z)\mathbf{g}. \quad (2)$$

Here, we use the hindrance function from [20]: $f(\phi) = \mu_l(1 - \phi)/\mu(\phi)$. The presence of a solid track at $z = 0$ is taken into account through $\omega(z) = A(z/d)^2 / \sqrt{1 + A^2(z/d)^4}$ [12]; $A = 1/18$ so that $\omega(z) \rightarrow 0$ as $z \rightarrow 0$, and $\omega \approx 1$ away from $z = 0$. We use this particular function $\omega(z)$ because it is an appropriate ap-

proximation for hinderance to settling of a single spherical particle due to the presence of a solid wall (a problem approached via method of images, see [12] for more details; A is a fitting parameter in the approximation). The settling model from [1], which omits this type of hinderance, overestimates the settling velocity of particles as one nears the solid track, resulting in settling rates which are not physically realistic. By including $\omega(z)$ in the model, we overcome this shortcoming of the settling model used in [1].

As noted in Introduction, two different approaches may be used to describe the effect of shear-induced migration. Since they result in similar expressions for migration flux, for simplicity, we follow the diffusion-based one. Hence, this effect is included in Eq. 1 through two separate terms, \mathbf{J}_{coll} and \mathbf{J}_{visc} . These terms are defined as in [22] and [23]. The net flux of particles due to irreversibility of collisions between pairs of particles is given by

$$\mathbf{J}_{coll} = -K_{coll} \frac{d^2}{4} (\phi^2 \nabla \dot{\gamma} + \phi \dot{\gamma} \nabla \phi). \quad (3)$$

The net flux due to gradients in viscosity, $\mu(\phi)$, is given as

$$\mathbf{J}_{visc} = -K_{visc} \frac{d^2}{4} \phi^2 \dot{\gamma} \frac{1}{\mu(\phi)} \frac{d\mu}{d\phi} \nabla \phi. \quad (4)$$

Here, K_{coll} and K_{visc} are proportionality constants determined from experiments. We follow [23] and use $K_{coll} = 0.41$ and $K_{visc} = 0.62$.

The fluxes given in Eqs. 2, 3 and 4 are all proportional to d^2 , a fact we have employed in §3, in our argument regarding the influence of particle size on settling behavior of particles. It is interesting to note that in Eq. 3, the first term in the brackets suggests that even if the particle distribution is uniform (i.e. $\nabla \phi = 0$), the migration will occur due to gradients in frequency of irreversible particle collisions. This migration will then induce gradients in ϕ and hence, the second term in the brackets of Eq. 3 is activated.

The governing equation given in 1 is accompanied by boundary conditions (zero normal flux at both $z = 0$ and $z = h$, where h is film thickness) and coupled to Navier-Stokes equations for liquid with viscosity $\mu(\phi)$. However, in order to gain insight into settling behavior of particles, it is sufficient to consider Eq. 1 at steady state [1]. Formally, we assume that the time scale of adjustment of ϕ in the z -direction is rapid. This approach is reasonable for describing settling behavior away from the contact line region and when the front has moved some distance down the incline, so that the flow may be assumed to be fully developed. It is therefore consistent with our experimental regime of studying the settling behavior. Assuming that the thin film is flat, the steady state is achieved when fluxes given in Eqs. 2, 3 and 4 balance in the z -direction

$$\mathbf{J}_{grav} + \mathbf{J}_{coll} + \mathbf{J}_{visc} = 0. \quad (5)$$

We also assume that the flow is simple and unidirectional, so that $\dot{\gamma} = \partial u / \partial z$. Henceforth, instead of using $\dot{\gamma}$, we revert to shear stress $\sigma = \mu(\phi) \dot{\gamma}$. By scaling Eq. 5 using $H \approx 1$ cm (typical film thickness) as the length scale in the z -direction and

$\rho_l g H \sin \alpha$ as the scale for σ , and integrating once, we arrive at the following ODE

$$\left[1 + \frac{2(K_{visc} - K_{coll})}{K_{coll}} \frac{\phi}{\phi_{max} - \phi} \right] \sigma \phi' = -\sigma' \phi - \frac{2\rho_s \cot \alpha}{9K_{coll}} (1 - \phi) \frac{Az^2}{\sqrt{\left(\frac{d}{H}\right)^4 + A^2 z^4}}, \quad (6)$$

where $\rho_s = (\rho_p - \rho_l) / \rho_l$. The assumption that the thin film is flat is equivalent to neglecting capillary effects; here, this assumption is justified since the appropriately defined capillary number is $Ca = (\rho_l g H^2 \sin \alpha) / (3\zeta) \approx 10$ (ζ is the surface tension of the liquid). Therefore, since the surface tension effects are neglected, the pressure in the suspension is hydrostatic, and the (scaled) gradient in shear stress is given as $\sigma' = -(1 + \rho_s \phi)$. The accompanying boundary conditions result from shear-stress balance at the free surface: $\sigma(0) = 1 + \rho_s \phi_0$ and $\sigma(1) = 0$, where we define $\phi_0 = \int_0^1 \phi dz$ [1]. In particular, the boundary condition at $z = 1$ results directly from the shear-stress balance, while a simple integration of σ' listed above (using the boundary condition at $z = 1$) yields $\sigma(0)$. We note that ϕ_0 is equivalent to the total amount of particles in a given column of suspension normal to the substrate. Hence, the boundary condition $\sigma(0)$ essentially enforces the conservation of total mass of particles in the column. Combining these expressions with Eq. 6 yields a system of ODEs and accompanying boundary conditions

$$\phi' = F(z, \phi, \sigma), \quad \sigma' = G(\phi), \quad (7a, b)$$

$$\sigma(0) = 1 + \rho_s \phi_0, \quad \sigma(1) = 0, \quad (8a, b)$$

where

$$F(z, \phi, \sigma) = \frac{1}{\sigma} \left[1 + \frac{2(K_{visc} - K_{coll})}{K_{coll}} \frac{\phi}{\phi_{max} - \phi} \right]^{-1} \times \left[(1 + \rho_s \phi) \phi - \frac{2\rho_s \cot \alpha}{9K_{coll}} (1 - \phi) \frac{Az^2}{\sqrt{\left(\frac{d}{H}\right)^4 + A^2 z^4}} \right], \quad (9)$$

and

$$G(\phi) = -(1 + \rho_s \phi). \quad (10)$$

This system may be solved numerically for $\phi(z)$ and $\sigma(z)$. In order to include regions of clear liquid or packed particles, we use $F(z, \phi, \sigma) = 0$ instead of Eq. 9 whenever $\phi(z) = 0$ or $\phi(z) = \phi_{max}$. The numerical solutions are discussed below. We also note that an identical system of equations for $\phi(z)$ and $\sigma(z)$ may be obtained directly from Eq. 1, by employing scaling arguments typical to thin film flows, and considering a flat film (see Appendix for details).

The system of equations for $\phi(z)$ and $\sigma(z)$ given by Eqs. 7 and 8 is solved numerically via a shooting method. The shooting is carried out from $z = 0$, using $\sigma(0)$ given by Eq. 8a) and adjusting $\phi(0)$ so that the numerical solution satisfies the boundary condition at $z = 1$, i.e., Eq. 8b). Since $\partial u / \partial z = \sigma(z) / \mu(\phi(z))$,

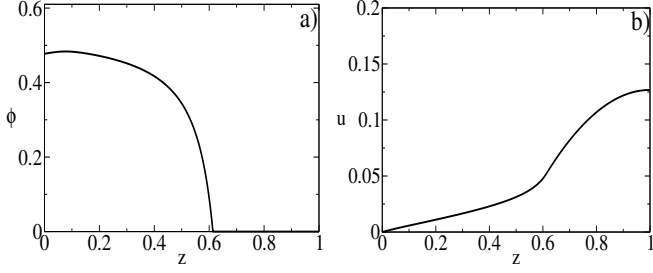


Figure 6: Numerical solution for $\phi_0 = 0.250$ and $\alpha = 15^\circ$: (a) particle volume fraction, $\phi(z)$; and (b) velocity, $u(z)$. Note that $\phi_{max} > \phi(0) > \phi_0$ and $\phi(1) = 0$. This corresponds to the *settled* regime.

once $\phi(z)$ and $\sigma(z)$ are known, $u(z)$ is readily found, by simply integrating once and using the no-slip boundary condition, $u(0) = 0$.

As previously noted in [1], when the wall-effect is neglected, due to the fact that σ is non-negative, ϕ is a monotonic function of z . This is because in such case $\mathcal{F} = \sigma F(z, \phi, \sigma)$, where $F(z, \phi, \sigma)$ is given by Eq. 9 with $Az^2 / \sqrt{(d/H)^4 + A^2z^4} = 1$, is a function of ϕ only, with a single unstable root $\bar{\phi}(\alpha)$ in the interval $(0, \phi_{max})$. Hence, either $\phi_{max} > \phi(0) > \phi_0$ and $\phi(1) = 0$, or $\phi(0) < \phi_0$ and $\phi(1) = \phi_{max}$, corresponding to experimentally observed settled and ridged regimes respectively. The well-mixed regime occurs when $\phi' = 0$ and $\phi(z) = \phi_0 = \bar{\phi}$ for $0 < z < 1$. Setting $\phi' = 0$, $\phi = \phi_0$ in Eq. 9 allows us to obtain an expression for the inclination angle corresponding to the well-mixed regime, α_{wm} , in terms of ϕ_0

$$\alpha_{wm} = \tan^{-1} \left[\frac{2\rho_s}{9K_{coll}} \frac{1 - \phi_0}{(1 + \rho_s\phi_0)\phi_0} \right]. \quad (11)$$

When the wall-effect is included, similar conclusions may be drawn based on the analysis of Eq. 9, and the settled and ridged regimes are recovered again. The well-mixed state is again unstable just like in the model without the wall-effect. However, the equivalent of Eq. 11 may not be written in closed form; the curve $\alpha_{wm}(\phi_0) = \alpha(\bar{\phi})$ is obtained numerically by seeking (ϕ_0, α) pairs which lead to the transition between settled and ridged outcomes when solving Eqs. 7 and 8. The resulting curves are shown as solid lines compared with the experimental results in the phase diagrams of Figs. 3, 4 and 5. The profiles for $\phi(z)$ and $u(z)$ obtained by numerically solving Eqs. 7-8 using several representative (ϕ_0, α) pairs are shown in Figs. 6, 7 and 8.

Figure 6 shows the profiles for $(\phi_0, \alpha) = (0.250, 15^\circ)$, corresponding to the settled regime in all phase diagrams in Figs. 3, 4 and 5. From Fig. 6a) it is evident this is the scenario where $\phi_{max} > \phi(0) > \phi_0$ and $\phi(1) = 0$. Most of the particles are in $z \leq 0.5$, after which ϕ decreases rapidly. Effectively, the particle-rich lower layer is covered by a less viscous clear liquid layer. Furthermore, in Fig. 6b), the velocity increases sharply for $z > 0.5$, causing clear liquid layer to flow faster than the particle-rich one. This is equivalent to the regime seen in Figure 2a) in which particles settled to the substrate and clear liquid continues down the track. In this case, the prediction of our model agrees well with the experimental results.

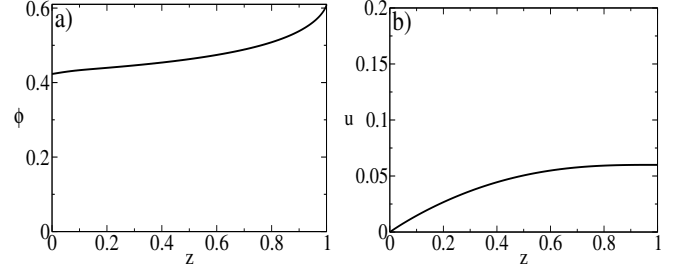


Figure 7: Numerical solution for $\phi_0 = 0.475$ and $\alpha = 45^\circ$: (a) particle volume fraction, $\phi(z)$; and (b) velocity, $u(z)$. Note that $\phi(0) < \phi_0$ and $\phi(1) = \phi_{max}$. This corresponds to the *ridged* regime.

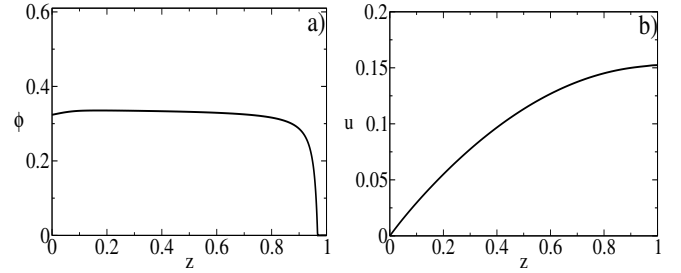


Figure 8: Numerical solution for $\phi_0 = 0.310$ and $\alpha = 45^\circ$: (a) particle volume fraction, $\phi(z)$; and (b) velocity, $u(z)$. Note that $\phi_{max} > \phi(0) > \phi_0$ and $\phi(1) = 0$ still apply.

In Fig. 7, the profiles for ϕ and u resulting from $(\phi_0, \alpha) = (0.475, 45^\circ)$ are given. We note that in all our experiments with these values of ϕ_0 and α , the ridged regime occurs (see Figs. 3, 4 and 5). Figure 7a) shows, in contrast to Fig. 6a), that $\phi(0) < \phi_0$ and $\phi(1) = \phi_{max}$. Therefore, particles aggregate close to the free surface of the film, and according to Fig. 7b), flow faster than the more dilute lower layer. This behavior is typical in the ridged regime observed in experiments and the model predictions are again in good agreement with our experimental results.

Finally, for $(\phi_0, \alpha) = (0.310, 45^\circ)$, the resulting ϕ and u profiles are given in Fig. 8. With the exception of experiments with the largest particles (see Fig. 4c)), this combination of ϕ_0 and α values leads to a well-mixed regime. From Fig. 8a), we see that for most of the film thickness, the particles are uniformly distributed. However, a close inspection reveals that this case still belongs to the category of solutions to Eqs. 7 and 8 where $\phi_{max} > \phi(0) > \phi_0$ and $\phi(1) = 0$, namely the settled regime. In addition, Fig. 8b) indicates that the very thin layer of clear liquid at the free surface still flows faster than the particle-laden layer below it. While our model is a steady state one, one could clearly see how in a dynamic setting the situation shown in Fig. 8 eventually leads to a settled regime, with the top layer of clear liquid becoming ever thicker and flowing ever faster as the system evolves.

Next, we examine the agreement between the numerically obtained $\alpha_{wm}(\phi_0)$ curve and the experimental results. We note that, apart from the inclusion of the hindrance due to the presence of a solid track in our model, another important difference between this study and the one in [1] is that we compare the predictions of our model to the results of much more extensive

experiments, involving several different liquid/particle combinations. For this purpose, we go back to Figs. 3, 4 and 5. In all diagrams, except the one in Fig. 4c), the curve lies completely within the well-mixed band, in excellent agreement with the experimental results. For largest particles in Fig. 4c), the well-mixed regime does not occur; however, the curve overlaps a large section of the border between settled and ridged bands marking the transition between these two regimes. This again hints at the transiency of the well-mixed regime. We already noted that the structure of Eqs. 7 and 8 indicates that the well-mixed regime is an unstable root of the system. Even if ϕ_0 and α values are adjusted to lie exactly on the well-mixed curve, even smallest perturbations eventually cause bifurcation to either settled or ridged regime. The strongest evidence for this argument is given by Fig. 4c), where relevant settling timescales are short enough so that bifurcation occurs rapidly and the well-mixed band simply collapses onto a well-mixed curve. Other phase diagrams in Figs. 3, 4 and 5 are also in line with our argument, only the timescales at which the bifurcation occurs are much longer compared to the one in Fig. 4c), leading to observable well-mixed regime. A sufficiently long experimental track would allow for bifurcation to occur, resulting in eventual collapse of all well-mixed bands in Figs. 3, 4 and 5.

Finally, it is worthwhile to emphasize that the presented model is a steady state one, while the behavior shown e.g., in Fig. 2a), where a clear film leaves a particle rich sediment behind and develops fingers, is clearly a dynamic process, which could only be captured by a more complete dynamic model. Consequently, the details of the transition between well-mixed and either of the two other regimes for a given liquid/particle combination may be captured with an inclusion of additional non-equilibrium effects. However, the settling behavior, which our simple model correctly predicts, is the most crucial ingredient, as it truly sets the stage for more complex dynamic processes. Therefore, this equilibrium model should be considered as one of the main components of any fully dynamic model.

5. Comparison of timescales

In this section we present an analysis of two relevant timescales in the dynamics – namely the timescale of the bulk flow and the timescale of settling to the substrate. The experimental data from the previous sections shows a pronounced ‘transient’ well-mixed regime in which the particles neither settle to the substrate nor towards the front of the flow on the timescale of the experiment. Fig. 4 shows that size of this regime (denoted by the light grey shaded area) depends dramatically on particle size – for the very small particles, Fig. 4 a), this is a large portion of the phase diagram, whereas for the largest particles, Fig. 4 c), we observe no transient regime. It is possible to develop some analysis of this problem based on simple timescales of the physics in the problem. We focus on the most dramatic changes in the data with respect to particle size – namely the shifting of the boundary between the well-mixed (light grey) and settled (white) regions, relative to the theoretical equilibrium prediction shown as a solid dark curve. We define two timescales for the problem: one for front motion down

the incline, denoted by T_f , and a timescale T_p on which particles settle towards the solid substrate. Both timescales involve bulk properties of the flow, although the T_f is largely insensitive to particle size, while T_p depends significantly on particle size. To accurately estimate these timescales we need to understand delicate details of the physics for this dynamic process, some of which is still not well understood. Nevertheless we show that with some basic scaling properties of the system we can gain some understanding of the experimental data presented here.

Naively, one might consider $T_f \sim L^3\nu/(\mathcal{A}^2g \sin \alpha)$ as used for clear liquid thin film flows [2], where \mathcal{A} is the cross-sectional area of the flow, and $T_p \sim H\nu/(d^2g \cos \alpha)$ based on the Stokes law. However, this approach oversimplifies the analysis. In fact, it contradicts the results in §3, which clearly indicate that settling due to gravity on its own is not sufficient to explain the experimental observations. Hence, we pursue a different route.

The timescale T_f is discussed in detail in the experimental paper [13] which considers the same experimental setup but focuses primarily on the well-mixed regime and the dynamics of the flow. In particular, based on the work for clear thin films in [2], in [13] it was argued that the dimensional quantity $C_N = t/X_N^3$, where t is time and X_N is front position, is constant in time for particle-laden thin films as well, at least when $\phi_0 \leq 0.45$ and $\alpha \leq 55^\circ$. This was shown by measuring C_N for various experimental configurations, using suspension volumes similar to those in our experiments. Here, it is appropriate to use their C_N data for L2/P1 configuration. Hence, our focus will be on the results in Figs. 4a) and b). More precisely, Huppert [2] derives the formula for a clear liquid from an exact similarity solution in which the position of the front is $X(t) = (9\mathcal{A}^2g \sin \alpha/4\nu)^{1/3}t^{1/3}$. Ward et al. [13] argue that for a range of parameters this same model holds with ν replaced by the effective viscosity of the mixture which depends on the bulk particle volume fraction. The data from [13] actually has quite good agreement with the model of Van Der Werff et al. [28] and Brady [29], $\mu(\phi) = \mu_L(1 - \phi_0/\phi_{max})^{-2}$, also known as the Krieger-Dougherty model. Based on the discussion so far, and noting that $\rho \propto (1 + \rho_s\phi_0)$, for a well-mixed thin film flowing down the incline we consider

$$T_f = \frac{C_f}{(1 - \phi_0/\phi_{max})^2(1 + \rho_s\phi_0) \sin \alpha}. \quad (12)$$

Here, the terms $(1 - \phi_0/\phi_{max})^{-2}$ and $(1 + \rho_s\phi_0)^{-1}$ appropriately include the dependence of T_f on the bulk particle volume fraction (via appropriate dependence on the suspension viscosity and density respectively); also $\rho_s = (\rho_p - \rho_l)/\rho_l \approx 1.5489$ and $\phi_{max} = 0.61$. The ‘mobility’ constant is $C_f = C_N L^3$, where $L = 0.9 \text{ m}$ is the length of the solid substrate; based on data from [13], $C_f \approx 1000 \text{ s}$.

As for T_p , rather than trying to understand the details of the dynamics of the fluxes, we write the simplest model that includes the following three effects:

1. The dependence of T_p on particle size. It must scale as d^{-2} because this scaling is present in both shear-induced migration and hindered settling.

2. The dependence of the settling time on bulk viscosity, as it depends on the bulk particle volume fraction.
3. The fact that for fixed values of ϕ_0 , $T_p \rightarrow \infty$ as $\alpha \rightarrow \alpha_{wm}$ because the particles do not settle if the hindered settling and shear-induced migration fluxes are in perfect balance.

This gives the following general model for T_p

$$T_p = \frac{C_p}{d^2(1 - \phi_0/\phi_{max})^2(1 + \rho_s\phi_0)} [\cos(\alpha + \pi/2 - \alpha_{wm})]^{-k}, \quad (13)$$

where k and C_p are positive constants. For simplicity we take $k = 1$. The proportionally constant C_p is estimated from the experimental data – so that $T_p = T_f$ at the boundary between well-mixed and settled regions, e.g., in Fig. 4a) for $\phi_0 = 0.37$; this gives $C_p \approx 0.136 \cdot 10^{-4} m^2 s$. We also note that for parameters near the well-mixed curve α_{wm} , $T_p \gg T_f$, because $T_p \rightarrow \infty$ as one approaches α_{wm} . Next, in the well-mixed region, $T_p > T_f$, while $T_p \approx T_f$ on the boundary with the settled regime. Finally, below the well-mixed region, we have that $T_p < T_f$.

Next we compare these timescales across different sets of experiments. For fixed values of ϕ_0 , we consider T_f and T_p as functions of α , such that $\alpha < \alpha_{wm}$. The influence of the particle size d on the position of the intersection between $T_f(\alpha)$ and $T_p(\alpha)$ is studied and the results are compared to experimental data in Figs. 4a) and b). We carry out this comparison for several different values of ϕ_0 for which we have detailed experimental data in Fig. 4, namely $\phi_0 = 0.31, 0.37$ and 0.425 (second, third and fourth column of data from the left). The results are given in Fig. 9. For all considered values of ϕ_0 , the intersection between T_f and T_p is an excellent indicator of the transition between settled and well-mixed regime for small particles P1. For medium size particles P2, the position of the intersection slightly overestimates the shrinking of the well-mixed region observed in experiments; nevertheless, the trend we see in Fig. 9 for P1 and P2 is consistent with our experimental data. These results further supports the notion of transiency of the well-mixed regime. The discussion in this section has focused on the transition from the well-mixed to settled regimes. We also note that there is a transition from the well-mixed regime to the particle-rich ridge. The latter is much less pronounced than the former, although it is visible in the data. A similar analysis could be performed to explain this transition as well.

6. Dynamic model

In §4, we show that the predictions of the equilibrium model agree well with the experimental data regarding different settling regimes. Here, we introduce a dynamic model which is motivated by the results of our equilibrium theory and lubrication models for clear liquid films. For lubrication models of clear liquids, to leading order the velocity profile in the z -direction is described by an equilibrium parabolic profile. Thus it is natural to consider a similar model for the particle-laden flow problem in which we assume an equilibrium profile in the z -direction given by a solution of the equilibrium equations (7-10). That is, given h and $\phi_0 = h^{-1} \int_0^h \phi(z) dz$ (and α of course), one may use the equilibrium model to obtain $\phi(z)$ and $u(z)$.

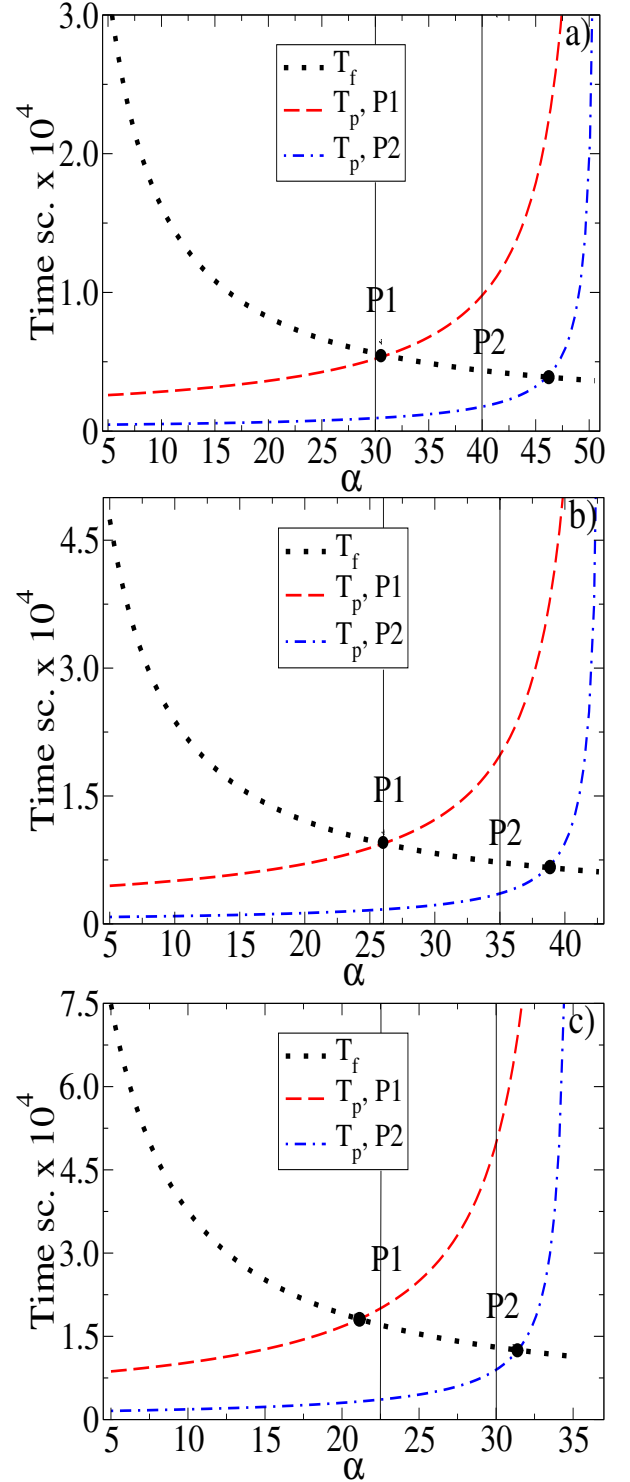


Figure 9: Comparison of $T_f(\alpha)$ and $T_p(\alpha)$ for small (P1) and medium size particles (P2) for a) $\phi_0 = 0.31$; b) $\phi_0 = 0.37$; and c) $\phi_0 = 0.425$. For given ϕ_0 , vertical lines indicate the value of α corresponding to the location of the boundary between well-mixed and settled regions in Fig. 4a), for P1, and Fig. 4b), for P2

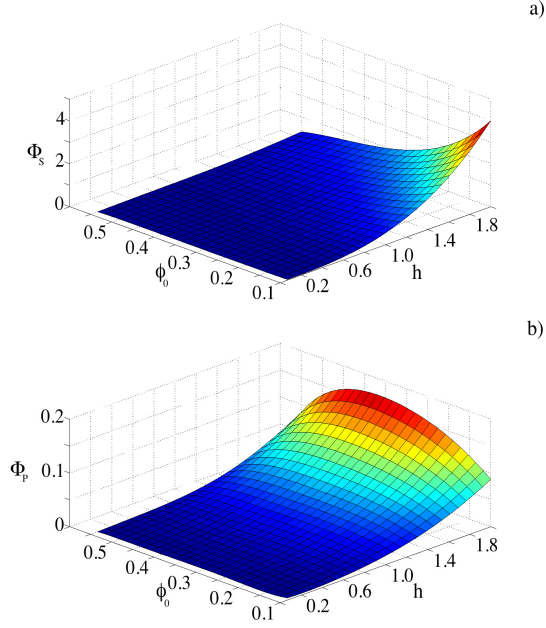


Figure 10: Suspension flux Φ_S in a), and particle flux Φ_P in b) as functions of h and ϕ_0 for $\alpha = 20^\circ$.

These profiles, in turn enable us to calculate two fluxes, namely the suspension flux and particle flux

$$\Phi_S = \int_0^h (1 + \rho_s \phi(z)) u(z) dz, \quad \Phi_P = \int_0^h \phi(z) u(z) dz \quad (14a, b)$$

respectively. We arrive at a dynamic model by using Φ_S and Φ_P to write two conservation laws, namely, conservation of suspension mass and particle mass

$$\frac{\partial}{\partial t} [(1 + \rho_s \phi_0) h] + \frac{\partial}{\partial x} [\Phi_S(h, \phi_0)] = 0, \quad (15)$$

$$\frac{\partial}{\partial t} [\phi_0 h] + \frac{\partial}{\partial x} [\Phi_P(h, \phi_0)] = 0, \quad (16)$$

respectively. This is a system of two scalar hyperbolic conservation laws.

Now, for a given α value, we must compute Φ_S and Φ_P as functions of h and ϕ_0 , using the equilibrium equations (7-10). These surfaces are given in Figs. 10 and 11 for two different α values. Both fluxes are smooth functions of h and ϕ_0 . Also, for small α , Φ_S is maximum when h is large and ϕ_0 is small (i.e. low viscosity case), see Fig. 10a). As α increases, another maximum develops for large h and intermediate values of ϕ_0 , see Fig. 11a), for which an increase in density (i.e., the $(1 + \rho_s \phi(z))$ term in Eq. 14a)) still overcomes the increase in suspension viscosity resulting from the presence of additional particles. On the other hand, Φ_P is always largest for large h and intermediate values of ϕ_0 . This is natural since for small ϕ_0 and large h the suspension flux is large, but there are very few particles carried with the flow, while when both ϕ_0 and h are large, the increase in viscosity severely hinders particle

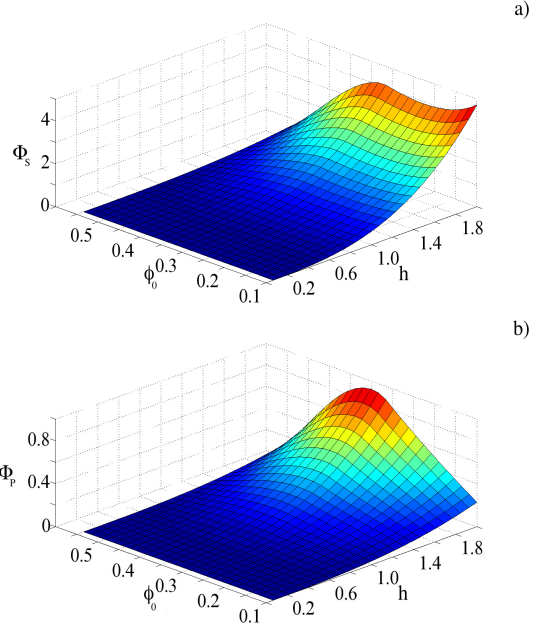


Figure 11: Suspension flux Φ_S in a), and particle flux Φ_P in b) as functions of h and ϕ_0 for $\alpha = 50^\circ$.

flux. The maximum increases in magnitude as α increases, see Fig. 10b) versus 11b).

Since these fluxes are smooth, we can easily fit them to a polynomial using least-squares. This is useful because it gives us a closed form expression for the fluxes in the equilibrium model rather than having to recompute these values for every timestep of the dynamic model. Here we use 5th order polynomials in h and ϕ_0 to fit to Φ_S and Φ_P . The system, Eqs. 15 and 16, is solved numerically using an upwind scheme. The initial conditions are step functions $h(x)$ and $\phi_0(x)$ similar to experimental profiles, i.e. h_{left} , h_{right} , ϕ_{0left} and ϕ_{0right} are given. We are careful in our choice of time-step in order to maintain stability of upwind scheme: we use $\Delta t < \Delta x/10$, a time-step perhaps smaller than needed since the CFL constant is difficult to calculate exactly for Eqs. 15 and 16. An example of the dynamic solution is shown in Fig. 12. It shows that the front motion in the settled case is predicted, at least qualitatively, rather well.

However, certain initial profiles $h(x)$ and $\phi_0(x)$ result in numerical instabilities no matter how small Δt we use. This can be understood by examining the hyperbolicity of the system given by Eqs. 15 and 16. In particular, we may rewrite Eqs. 15 and 16 as

$$\left| \begin{array}{c} (1 + \rho_s \phi_0) h \\ \rho_0 h \end{array} \right|_t + \mathbf{J} \left| \begin{array}{c} (1 + \rho_s \phi_0) h \\ \rho_0 h \end{array} \right|_x = 0,$$

where

$$\mathbf{J} = \left| \begin{array}{cc} \frac{\partial \Phi_S}{\partial h} - \frac{\phi_0}{h} \frac{\partial \Phi_S}{\partial \phi_0} & \frac{1}{h} (1 + \rho_s \phi_0) \frac{\partial \Phi_S}{\partial \phi_0} - \rho_s \frac{\partial \Phi_S}{\partial h} \\ \frac{\partial \Phi_P}{\partial h} - \frac{\phi_0}{h} \frac{\partial \Phi_P}{\partial \phi_0} & \frac{1}{h} (1 + \rho_s \phi_0) \frac{\partial \Phi_P}{\partial \phi_0} - \rho_s \frac{\partial \Phi_P}{\partial h} \end{array} \right|.$$

The system remains hyperbolic if and only if

$$\left(\frac{\phi_0}{h} \frac{\partial \Phi_S}{\partial \phi_0} - \frac{\partial \Phi_S}{\partial h} + \rho_s \frac{\partial \Phi_P}{\partial h} - \frac{1}{h} (1 + \rho_s \phi_0) \frac{\partial \Phi_P}{\partial \phi_0} \right)^2 \geq$$

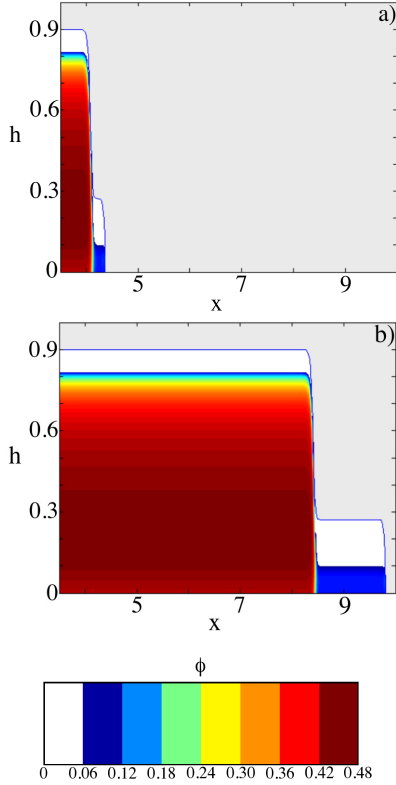


Figure 12: Evolution of the particle-laden thin film predicted by the system of hyperbolic conservation laws, Eqs. 15 and 16, with $\alpha = 20^\circ$, shown at $t = 5$ in a), and $t = 25$ in b). Here, $(h_{left}, h_{right}) = (0.9, 0.05)$ and $(\phi_{0_{left}}, \phi_{0_{right}}) = (0.3, 0.075)$. The h profiles are shown; the color scheme is produced by running the resulting h and ϕ_0 as inputs to our equilibrium model, Eqs. 7-10, and represents $\phi(z)$ profiles for each x -position.

$$\frac{4}{h} \left(\frac{\partial \Phi_S}{\partial h} \frac{\partial \Phi_P}{\partial \phi_0} - \frac{\partial \Phi_S}{\partial \phi_0} \frac{\partial \Phi_P}{\partial h} \right). \quad (17)$$

The regions where hyperbolicity of Eqs. 15 and 16 fails is shown in Fig. 13 for the situation corresponding to $\alpha = 50^\circ$. It indicates that the system fails to be hyperbolic when both h and ϕ_0 are large, but surprisingly it is hyperbolic as $\phi_0 \rightarrow \phi_{max}$. Furthermore, it is unexpected that small values of h , where some of the assumptions used in deriving our continuum models may be violated, are not problematic. The fin-like region of hyperbolicity loss for relatively small ϕ_0 and intermediate values of h is also difficult to connect to any immediately obvious physical mechanism.

The dynamic model shows some promise, however, before we can proceed with detailed comparison with experimental data, the issue of loss of hyperbolicity requires better understanding. Further work will examine the details of the fitting approach for fluxes Φ_S and Φ_P [30].

7. Conclusions

In this paper, we focus on experiments with particle-laden thin film flows down an incline, where the effects of the viscosity of the suspending liquid and the particle size are examined. We observe that the settling behavior of particles proceeds

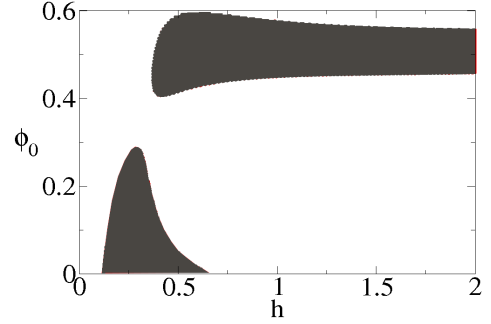


Figure 13: Hyperbolicity of the system of conservation laws, Eqs. 15 and 16, for $\alpha = 50^\circ$. The regions where the system loses hyperbolicity are shown in grey.

in three distinct regimes: settled, well-mixed, and ridged, depending on the bulk volume fraction, ϕ_0 , and the inclination angle, α . Our theoretical model, based on an equilibrium theory, where the hindered settling balances the shear-induced migration, is found to be in an excellent agreement with our experimental data. More precisely, its predictions for the transition between the settled and the ridged regime match the experimental observations exactly over all ranges of viscosities and particle sizes. Furthermore, both our model and our experimental results suggest that the intermediate well-mixed regime is a transient. In particular, our equilibrium theory predicts no such regime; our experiments show how the well-mixed band collapses as the relevant timescales are changed by varying the viscosity and the particle size. Therefore, we argue that the well-mixed regime eventually leads to a bifurcation to either the settled or the ridged regime.

Our experimental results indicate that the particle size is a significant parameter. The likelihood of observing the well-mixed regime increases with the decrease in the particle diameter. The viscosity of the suspending liquid is found to affect the relevant timescale of the flow. For the smallest considered particle size, the liquid viscosity also significantly affects the likelihood of the well-mixed regime: it is more prevalent in the case of a less viscous suspending liquid. A combination of a low viscosity liquid and small particles significantly affects the relevant timescales; the flowing film runs out of track length before any substantial disturbance to the uniformity of the suspension is observed. The viscosity of the suspending liquid most likely also affects the length scale over which the transition from the uniform state occurs – particularly the transition to the settled regime. Namely, larger viscosity results in a longer time scale on which the balance of the particle fluxes in the z -direction occurs, leading to a larger length scale of the flow needed to observe this balance. We argue that given a sufficiently long track, the well-mixed bands in phase diagrams such as those in Figs. 3, 4 and 5 might eventually collapse onto a well-mixed line predicted by our model, so that only the settled and the ridged regimes are observed.

Our results, both experimental and theoretical, are novel in several aspects. The influence of the particle size and the liquid viscosity on the observed settling regime has not been studied previously. Also, the manner in which these two material pa-

rameters affect the well-mixed regime, as well as the implications related to transiency of this regime are also novel. Finally, our theoretical model improves on the previously used steady-state models by incorporating an additional hinderance effect, thereby leading to physically realistic settling predictions.

This paper makes a significant step towards a fully quantitative model by identifying the dominant equilibrium physics for the flow. In addition, it also implies further modifications required in order to fully understand the transiency of the well-mixed regime and the intricacies connected to the timescales relevant to the front motion and particle settling. We take it a step further and use the results from the equilibrium model in deriving a dynamic model based on a system of scalar hyperbolic conservation laws. Our preliminary results indicate this model shows some promise in describing the front motion in particle-laden thin film flows. We hope to improve this model and build ever more sophisticated dynamic models based on it. Our study also raises interesting questions regarding the motion of the contact lines and the fingering instability. A more complete theoretical model would allow for a comparison with the time dependent experimental results from [13], regarding the front motion in particle-laden films. In addition, the experiments with clear liquid flows in [5] showed that once the fingering instability occurred, the exponent in the power law from [2] describing the evolution of the front position was modified. Carrying out a similar study in the particle-laden setting would indeed be compelling, especially since it would also allow for examination of the connection between different settling regimes and the wavelength of the fingering instability. The relationship between the motion of the particulate bed in the settled case and the properties of the solid surface is also of interest. Finally, more sophisticated experimental equipment would also allow for PIV measurements and reveal the details of the particle motion. This would, in turn, lead to a full quantitative resolution of volume fraction profiles close to the free surface and the solid in the ridged and settled regimes respectively.

Acknowledgements

The authors would like to gratefully acknowledge the helpful comments of Benjamin Cook, Dirk Peschka, and Benoit Pausader. The bulk of the experimental work presented here was carried out during the Research Experience for Undergraduates (REU) program at University of California, Los Angeles during Summer 2009. We thank Samantha Mesuro and Jake Bouricius for providing the data shown in Fig. 12. This work was supported by NSF grants DMS-0601395 and DMS-1048840, and the UC Lab research fund 09-LR-04-116741-BERA.

A. Appendix

Here, we give an alternate approach for deriving Eqs. 7-10 (i.e. the system of ODEs for ϕ and σ) directly from the dynamic equation for ϕ , Eq. 1. In fact, this system arises from a general framework one may employ for studying the contact line stability, consisting of the Navier-Stokes equations and accompanying boundary conditions, coupled with Eq. 1, when flat

film assumption is employed. First, the expressions for particle fluxes due to the hindered settling and the shear-induced migration, Eqs. 2-4, are substituted into Eq. 1. Assuming $\mu(\phi)$ is given as in §4, and $\dot{\gamma} = \partial u / \partial z$, Eq. 1 becomes

$$\begin{aligned} \phi_t + u\phi_x + w\phi_z = & \frac{d^2 K_{coll}}{4} \nabla \cdot \phi \left| \begin{array}{c} (u_z \phi)_x \\ (u_z \phi)_z \end{array} \right| + \\ & \frac{d^2 K_{visc}}{2} \nabla \cdot \frac{\phi^2 u_z}{\phi_{max} - \phi} \left| \begin{array}{c} \phi_x \\ \phi_z \end{array} \right| + \\ & \frac{d^2 \rho_s \rho_l g}{18 \mu_l \phi_{max}^2} \nabla \cdot \phi (1 - \phi) (\phi_{max} - \phi)^2 \omega(z) \left| \begin{array}{c} \sin \alpha \\ \cos \alpha \end{array} \right|, \end{aligned} \quad (18)$$

where $\nabla = (\partial x, \partial z)$. Next, we scale Eq. 18 using the time, length, and velocity scales typically utilized for thin film flows (e.g., see [11]). While surface tension will eventually be neglected, at this point, the small parameter is $\epsilon = (3Ca)^{1/3}$, where the capillary number Ca is defined as before. The scale in the z -direction is H , and the one in the x -direction is H/ϵ ; u is scaled using $u_{sc} = (H^2 \rho_l g \sin \alpha) / (3\mu_l)$, while w is scaled using ϵu_{sc} ; the timescale is given as $H / (\epsilon u_{sc})$. In addition, we assume that $\phi \sim O(1)$. To the leading order in ϵ , we obtain

$$\begin{aligned} & K_{coll} \left(\phi (u_z \phi)_z \right)_z + 2K_{visc} \left(\frac{\phi^2 u_z}{\phi_{max} - \phi} \phi_z \right)_z + \\ & \frac{2\rho_s \cot \alpha}{3\phi_{max}^2} \left(\phi (1 - \phi) (\phi_{max} - \phi)^2 \frac{Az^2}{\sqrt{\left(\frac{d}{H}\right)^4 + A^2 z^4}} \right)_z = 0. \end{aligned} \quad (19)$$

We proceed by substituting $u_z = 3(1 - \phi/\phi_{max})^2 \sigma$ and integrating Eq. 19 with respect to z ; a simple manipulation yields Eq. 6. Next, the Navier-Stokes equations and the accompanying shear-stress balance at the free surface are scaled using identical scales and leading-order terms in ϵ are considered. If, for a moment, we assume that the film is locally flat, the effect of surface tension drops out of the shear-stress balance. Finally, this assumption leads to $\sigma' = -(1 + \rho_s \phi)$, and hence, Eqs. 7-10 as before.

References

- [1] B. P. Cook, Theory for particle settling and shear-induced migration in thin-film liquid flow, *Phys. Rev. E* 78 (2008) 045303.
- [2] H. Huppert, Flow and instability of a viscous current down a slope, *Nature* 300 (1982) 427.
- [3] N. Silvi, E. B. Dussan V., On the rewetting of an inclined solid surface by a liquid, *Phys. Fluids* 28 (1985) 5.
- [4] S. M. Troian, E. Herbolzheimer, S. A. Safran, J. F. Joanny, Fingering instabilities of driven spreading films, *Europhys. Lett.* 10 (1989) 25.
- [5] J. M. Jerrett, J. R. de Bruyn, Finger instability of a gravitationally driven contact line, *Phys. Fluids A* 4 (1992) 234.
- [6] L. Kondic, A. L. Bertozzi, Nonlinear dynamics and transient growth of driven contact lines, *Phys. Fluids* 11 (1999) 3560.
- [7] L. Kondic, Instability in the gravity driven flow of thin liquid films, *SIAM Review* 45 (2003) 95.
- [8] Y. Nohguchi, K. Hutter, S. B. Savage, Similarity solutions for granular avalanches of finite mass with variable bed friction, *Continuum Mech. Thermodyn.* 1 (1989) 239.

- [9] S. B. Savage, K. Hutter, The motion of a finite mass of granular material down a rough incline, *J.Fluid Mech.* 199 (1989) 177.
- [10] O. Pouliquen, J. Delour, S. B. Savage, Fingering in granular flow, *Nature* 386 (1997) 816.
- [11] J. J. Zhou, B. Dupuy, A. L. Bertozzi, A. E. Hosoi, Theory for shock dynamics in particle-laden thin films, *Phys. Rev. Lett.* 94 (2005) 117803.
- [12] B. P. Cook, A. L. Bertozzi, A. E. Hosoi, Shock solutions for particle-laden thin films, *SIAM J.Appl. Math.* 68 (2007) 760.
- [13] T. Ward, C. Wey, R. Glidden, A. E. Hosoi, A. L. Bertozzi, Experimental study of gravitation effects in the flow of a particle-laden thin film on an inclined plane, *Phys. Fluids* 21 (2009) 083305.
- [14] J. F. Richardson, W. N. Zaki, The sedimentation of a suspension of uniform spheres under conditions of viscous flow, *Chem. Eng. Sci.* 3 (1954) 65.
- [15] G. K. Batchelor, Sedimentation in a dilute suspension of spheres, *J.Fluid Mech.* 52 (1972) 245.
- [16] E. Barnea, J. Mizrahi, A generalized approach to the fluid dynamics of particulate systems 1. General correlation for fluidization and sedimentation in solid multiparticle systems, *Chem. Eng. J.* 5 (1973) 171.
- [17] R. Buscall, J. W. Goodwin, R. H. Ottewill, T. F. Tadros, The settling of particles through Newtonian and non-Newtonian media, *J. Colloid Interface Sci.* 85 (1982) 78.
- [18] R. H. Davis, A. Acrivos, Sedimentation of noncolloidal particles at low Reynolds-numbers, *Ann. Rev. Fluid Mech.* 17 (1985) 91.
- [19] P. Snabre, P. Mills, Settling and fluidization of non-Brownian hard spheres in a viscous liquid, *Euro. Phys. J. E* 1 (2000) 105.
- [20] U. Schafflinger, A. Acrivos, K. Zhang, Viscous resuspension of a sediment within a laminar and stratified flow, *Int. J.Multiphase Flow* 16 (1990) 567.
- [21] D. Leighton, A. Acrivos, Measurement of shear-induced self-diffusion in concentrated suspensions of spheres, *J.Fluid Mech.* 177 (1987) 109.
- [22] D. Leighton, A. Acrivos, The shear-induced migration of particles in concentrated suspensions, *J.Fluid Mech.* 181 (1987) 415.
- [23] R. J. Phillips, R. C. Armstrong, R. A. Brown, A. L. Graham, J. R. Abbott, A constitutive equation for concentrated suspensions that accounts for shear-induced particle migration, *Phys. Fluids A* 4 (1992) 30.
- [24] J. M. Kim, S. G. Lee, C. Kim, Numerical simulations of particle migration in suspension flows: Frame-invariant formulation of curvature-induced migration, *J. Non-Newtonian Fluid Mech.* 150 (2008) 162.
- [25] P. R. Nott, J. F. Brady, Pressure-driven flow of suspensions - simulation and theory, *J.Fluid Mech.* 275 (1994) 157.
- [26] J. F. Morris, F. Boulay, Curvilinear flows of noncolloidal suspensions: The role of normal stresses, *J.Rheology* 43 (1999) 1213.
- [27] B. D. Timberlake, J. F. Morris, Particle migration and free-surface topography in inclined plane flow of a suspension, *J.Fluid Mech.* 538 (2005) 309.
- [28] J. C. Van Der Werff, C. G. De Kruif, Hard-sphere colloidal dispersions: The scaling of rheological properties with particle size, volume fraction, and shear rate, *J. Rheol.* 33 (3).
- [29] J. F. Brady, The rheological behavior of concentrated colloidal dispersions, *J. Chem. Phys.* 99 (1).
- [30] A. Bertozzi, N. Murisic, B. Pausader, D. Peschka, A dynamic model for resuspension in particle laden flow (2011).